Soft Matter

PAPER

View Article Online
View Journal | View Issue

Cite this: *Soft Matter*, 2024, **20**, 5122

Hydrogel–tissue adhesion by particle bridging: sensitivity to interfacial wetting and tissue composition†

Raphaël Michel *[ab] and Laurent Corté *[ac]

Solid particles placed at the interface between hydrogels and biological tissues can create an adhesive joint through the adsorption of macromolecules onto their surfaces. Here, we investigated how this adhesion by particle bridging depends on the wetting of tissue surfaces and on the heterogeneities in tissue composition. *Ex vivo* peeling experiments were performed using poly(ethylene glycol) films coated with aggregates of silica nanoparticles deposited on the internal tissues of porcine liver. We show that the adhesion produced by particle bridging is altered by the presence of fluid wetting the tissue–hydrogel interface. For both uncoated and coated films, a transition from lubricated to adhesive contact was observed when all the interfacial fluid was drained. The presence of a silica nanoparticle coating shifted the transition towards more hydrated conditions and significantly enhanced adhesion in the adhesive regime. After 5 min of contact, the adhesion energy achieved on liver parenchyma with the coated films (7.7 ± 1.9 J m^{-2}) was more than twice that of the uncoated films (3.2 ± 0.3 J m^{-2}) or with a surgical cyanoacrylate glue (2.9 ± 1.9 J m^{-2}). Microscopic observations during and after peeling revealed different detachment processes through either particle detachment or cohesive fracture in the tissue. These mechanisms could be directly related to the microanatomy of the liver parenchyma. The effects of both interfacial wetting and tissue composition on adhesion may provide guidelines to tailor the design of tissue adhesives using particle bridging.

Received 6th March 2024,
Accepted 3rd June 2024

DOI: 10.1039/d4sm00287c

rsc.li/soft-matter-journal

1. Introduction

Particle bridging consists in placing solid particles at the interface between two pieces of polymer gels to create adhesion.[1] Binding between the two pieces occurs when numerous polymer strands from both gels adsorb onto the particles which then act as connectors across the interface. This effect was demonstrated in the case of polymer hydrogels using nanoparticles (NPs) or microscopic aggregates of nanoparticles.[1–4] Interestingly, it can also be applied to create adhesion to biological tissues which are composed of hydrated networks of biomacromolecules. In their seminal study, Rose *et al.* achieved *ex vivo* adhesion by gluing two pieces of calf liver with a solution of silica nanoparticles.[1] An *in vivo* study by Meddahi-Pelé *et al.* on rat models showed that poly(vinyl alcohol)- and polysaccharide-based hydrogel membranes coated with aggregates of silica NPs adhered within a minute to the bleeding surface of a resected liver as well as to the surface of a beating heart.[5] Following these works, several studies have investigated the adhesion to biological tissues by particle bridging using various types of particles such as silica,[3–8] bioactive glass,[9,10] silicon[11] and diverse metal oxides.[5,9] Particles were designed to combine the particle bridging effect with other functionalities such as antibacterial[6] and antioxidant properties[8] as well as enhanced contrast for medical imaging.[7,11] Such tissue adhesives could be of practical interest for a large array of biomedical applications including hemostasis,[12] wound dressing[12,13] or topical drug and cell delivery.[14] Nevertheless, for these applications, the design of efficient particle bridging adhesives is greatly challenged by the wet conditions of the contact area, which may hinder the adsorption of polymer strands, and by the variability and heterogeneity of the tissue composition, which may require a specific design of particle surfaces for each case. In this work, we explored these two effects using model *ex vivo* peeling experiments.

One major difficulty in creating adhesion onto biological tissues arises from the fact that living tissues are highly hydrated. Living tissue surfaces are submitted to a continuous

[a] *Molecular, Macromolecular Chemistry, and Materials, ESPCI Paris, CNRS, PSL University, 10 rue Vauquelin, 75005, Paris, France. E-mail: raphael.michel@cermav.cnrs.fr*
[b] *Université Grenoble Alpes, CNRS, CERMAV, 38000 Grenoble, France*
[c] *Centre des Matériaux, MINES Paris, CNRS, PSL University, 63-65 rue Henri-Auguste Desbruères, 91003, Evry, France. E-mail: laurent.corte@minesparis.psl.eu*

† Electronic supplementary information (ESI) available. See DOI: https://doi.org/10.1039/d4sm00287c

wetting that dilutes possible reactive moieties and prevents molecular interactions across the interface. Adhesion can be promoted by draining the interfacial fluid and dehydrating the tissues. This effect was first reported in the case of mucoadhesion. Studies by Smart and coworkers showed how adhesion to the mucus increases with local mucus dehydration.[15,16] More recently, we showed through peeling experiments of hydrogel membranes on porcine liver tissues, that the capacity of the hydrogel to drain the interfacial fluid is a key factor to achieve adhesion onto tissues.[17] A model describing the competition between wetting of the interface by tissue fluids and draining of the interface by hydrogel swelling captured the transition from a lubricated to an adhesive contact. In a separate study, Yuk *et al.* further combined these interfacial draining and tissue dehydration effects using appropriate surface chemistry to design superabsorbant double-sided tapes with remarkable *in vivo* tissue adhesive performances.[18] In the case of particle bridging, little is known about the sensitivity toward wet conditions. However, pull-off tests on the capsule of porcine liver using hydrogel patches coated with silica nanoparticles showed a five-fold drop in adhesion strength when comparing *ex vivo* to *in vivo* conditions.[19] This effect most likely arises from differences in tissue hydration and strongly suggests that particle bridging onto tissues is altered by interfacial wetting.

Another critical consideration is the sensitivity of particle bridging to the tissue composition. The surface of biological tissues has complex macro- and microscopic morphologies with heterogeneous composition and mechanical properties. Therefore, heterogeneities in the tissue may lead to heterogeneities in the adhesive properties. This is well illustrated by studies using bare hydrogels (without interfacial NPs) on different tissues (*i.e.* from different organs).[20,21] In these cases, a single hydrogel system exhibits dissimilar adhesive performances depending on the nature of the tissue substrate. Building on this observation, it has been shown that tuning the chemistry of a gel, for instance by increasing the density of certain chemical functions (aldehyde), can improve its adhesive performance on a given tissue.[20,22] This underlines the necessity of adapting the hydrogel chemistry to the specific tissue composition. Therefore, in the case of adhesion by particle bridging, it appears necessary to define which part of the tissue preferentially adheres to the particles in order to improve their adhesive role.

Here, we address these questions experimentally using an *ex vivo* system to measure the adhesion produced by silica nanoparticle aggregates placed at the interface between poly(ethylene glycol) (PEG) films and porcine liver tissues. These aggregates of silica nanoparticles are similar to the ones used in previous *ex vivo* and *in vivo* studies.[19] The cross-linked PEG films were specifically formulated to display an almost purely elastic behaviour. Therefore, the dissipation in the bulk of the film during the debonding process is negligible and the measured work of adhesion corresponds mainly to the mechanisms occurring near the interface. Adhesion testing was performed on porcine liver which is commonly used to assess the properties of surgical adhesives.[7,18,19,21] It is a particularly challenging substrate and the reported adhesion values are usually substantially lower than the ones obtained on other organs such as the heart or the small intestine.[18,21] We focus on the mechanisms of particle bridging onto the internal tissues of porcine liver, referred to here as parenchyma. These internal tissues exhibit a microanatomy consisting of adjacent structural units called the liver lobules that have a polygonal shape with a characteristic size varying from 1 mm to 2.5 mm.[23,24] Two types of tissues compose this lobular structure: (i) the lobule interior made of a porous cellular tissue containing mostly hepatocytes with a variety of other cells (Kupfer cells, endothelial cells and stellate cells) forming a porous network of blood and bile vessels[23] and (ii) the lobular walls also called connective tissue septa that surround the lobules and are essentially made of extracellular matrix proteins (collagen type I, III and IV, and fibronectin).[25] Upon contact with coated PEG films, these heterogeneities in composition may lead to distinct interactions with the nanoparticles and yield different local adhesive behaviours. Using porcine hepatic parenchyma as an *ex vivo* model also gives us the possibility to precisely adjust the hydration of superficial tissue layers by immersing liver samples in physiological serum for a specific time.[17] In the following, experiments were performed on liver substrates with varying water content so as to probe the influence of tissue hydration on the adhesive performance of NP-coated hydrogels. Due to the absence of tissue vascularization, *ex vivo* adhesion with long contact times is expected to be less representative of the *in vivo* conditions. For this reason, we were primarily interested in probing short contact times. The sensitivity to tissue composition was investigated *via* microscopic observations of the detachment mechanisms during peeling.

The present study first reveals that adhesion by particle-bridging is altered on highly hydrated tissues for which interfacial wetting prevents molecular contact. Depending on the ability of the NP-coated films to drain interfacial fluids, lubricated or adhesive contact may be achieved. Additionally, we find that the capillary absorption of fluids within the porosities of the NP-coating contribute to interfacial draining and thus improve the adhesive performance in moderately hydrated conditions. Secondly, our experiments demonstrate that the strength of the particle bridging mechanism varies with the local composition and nature of the tissues. On heterogeneous tissues like the liver parenchyma, the joint formed by tough collagen-rich tissues adsorbed onto the silica NP-coating constitute the main contribution to the recorded adhesion strength while fragile cellular tissues remain adsorbed on the silica NP-coating and break cohesively upon detachment.

2. Experimental section

2.1. Materials

Sodium chloride ($\geq$99%), ethanol ($\geq$99.8%), pentaerythritol tetrakis (3-mercaptopropionate) (QT, $\geq$95%), poly(ethylene glycol) diacrylate (PEGDA, M_n = 700 kg mol^{-1}) and a colloidal silica suspension (Ludox® TM-50) were purchased from Sigma-Aldrich.

Triethylamine (TEA, ≥99%), 1,6-hexanedithiol (HT, 97%), ammonia solution ($NH_3{\cdot}H_2O$, 28%) and tetraethyl orthosilicate (TEOS) were purchased from Alfa Aesar. A surgical cyanoacrylate glue (GLUture®) containing 60% 2-octyl cyanoacrylate and 40% *N*-butyl cyanoacrylate, was purchased from Zoetis. Unless otherwise specified, all these chemicals were used as purchased without further purification.

2.2. Porcine liver harvesting and storage

Porcine liver tissues were obtained from two different sources. (i) Freshly dissected livers were harvested from freshly killed 3-month-old pigs (Sus scrofa domesticus, approx. 25 kg) at the Ecole de Chirurgie du Fer-à-Moulin (AP-HP) (7 Rue du Fer À Moulin, 75005, Paris, France) in accordance with the principles of animal care. Whole livers were transported in a cooler and were stored at 4 °C in physiological serum. They were used between 2 and 30 hours following their harvesting. (ii) Drained pig livers were purchased from a local butcher shop (59 rue Monge, 75005 Paris, France). Drained livers were transported in a cooler and stored at 4 °C. They were used during the 3 days following their purchase (18–76 hours after harvesting). These livers were not stored in the freezer as this is known to alter their integrity.[26]

2.3. Fabrication and characterization of PEG films

Cross-linked PEG films were prepared as previously reported.[17] Poly(ethylene glycol)diacrylate (PEGDA) was cross-linked with a mixture of hexanedithiol (HT) and pentaerythritol tetrakis(3-mercaptopropionate) (QT) in 15 wt% ethanol and triethylamine (TEA) was used as a catalyst (molar ratio PEGDA/HT/QT: 24/22/1). The concentration of TEA was adjusted to account for 1 mol% of thiol groups. PEGDA, HT and the corresponding fraction of TEA were first mixed at 21 °C and left to react under stirring (150 rpm) until conversion of 90% of the acrylate groups was achieved, as confirmed by infrared spectroscopy. QT, ethanol, and the remaining TEA were then added to the mixture and further stirred for 10 minutes. The mixture was injected in rectangular glass molds of 100 mm × 80 mm × 1.1 mm. The molds were sealed with silicone and stored for 5 days at room temperature (20 ± 2 °C). After removal from the molds, the hydrogel films were vacuum-dried until complete evaporation of the ethanol and triethylamine. They were then thoroughly washed by immersion (>3 h) in ultrapure water to eliminate the extractible soluble fraction (<0.1 wt%). The washed hydrogel membranes were subsequently dried in an oven at 60 °C until complete water evaporation. The resulting dry PEG films had a thickness of 1 ± 0.03 mm. The swelling ratio defined as the ratio of the swollen mass over the dry mass at equilibrium in water at room temperature was measured to be Q_{eq} = 2 and was reached after 3 hours of immersion (see Fig. S1, ESI†).

2.4. Preparation and characterization of silica nanoparticle coatings

2.4.1. Nanoparticle size measurements. Nanoparticle size was measured by Dynamic Light Scattering (DLS) using an ALV/CGS-3 Compact Goniometer system with an ALV/LSE-5004 multiple tau digital correlator (ALV, Langen, Germany), using a 90° scattering geometry and a 632 nm laser diode. All experiments were carried out in a thermostatic bath at 25 ± 0.1 °C. Nanoparticle solutions were diluted down to 0.01 wt% before the measurement to avoid multiple scattering. The mean hydrodynamic radius of the particles was evaluated using the cumulant method.[27]

2.4.2. Nanoparticle aggregation. Aggregates of nanoparticles were obtained from Ludox® TM-50 solutions composed of a colloidal suspension of silica particles with a diameter of 30 nm, as measured by DLS. The as-purchased solutions were dialyzed for two days against 1 L of ultrapure water using VISKING® dialysis tubes (Carl Roth, molecular weight cut-off: 12–14 kDa), renewing the water at least five times during this period. A powder of microscopic nanoparticle aggregates was obtained as follows. First, a small volume of the particle solution (10 to 20 mL) was left to dry in an oven at 80 °C until complete solvent evaporation (less than 1 mg variation in dry extract mass between two consecutive 4 h drying steps). The solid aggregates were then ground in an agate mortar and the powder was sieved through a 63-μm mesh size aluminium sieve.

2.4.3. Fluorescent nanoparticle aggregates. Fluorescent aggregates were prepared by introducing a small quantity of fluorescent silica nanoparticles to the dialyzed Ludox® TM-50 particle suspension. The fluorescent particles were synthesized using the Stöber method in the presence of a fluorescent tris(bipyridine)ruthenium(II) chloride complex ($[Ru(bpy)_3]Cl_2$) with a maximum excitation wavelength of 458 nm and a maximum emission wavelength of 595 nm.[28] For this, ethanol (300 mL) and ammonium hydroxide (19 mL) were first mixed together by stirring for 15 minutes at room temperature. TEOS (24 mL) was then added and the resulting mixture was left under stirring. After 3 hours, an aqueous solution of $[Ru(bpy)_3]Cl_2$ (20 mL at 15 mg mL^{-1}) was poured into the mixture which was further left under stirring for 24 hours. The resulting solution, containing large fluorescent particles with a diameter of about 600 nm as measured by DLS, was dialyzed 5 times against 1 L of ultrapure water. Finally, a small volume of this solution was added to a dialyzed Ludox® TM-50 particle suspension so that the final mass of the fluorescent particles accounted for 1% of the total silica mass. This final solution was left to dry in an oven at 80 °C until complete solvent evaporation and the solid aggregates were ground and sieved using the same protocol as in the case of non-fluorescent coatings.

2.4.4. Coating and glue deposition. Coatings of silica nanoparticle aggregates were produced by depositing an excess of nanoparticle powder on the surface of the dry PEG films (4 mg cm^{-2}). The powder was spread with a brush and the excess powder, which did not adhere to the PEG, was brushed away. Aggregates were left to adsorb onto the films for 5 min before contact was made with the liver. In the case of the surgical cyanoacrylate glue GLUture®, a few drops of glue were deposited and spread on the PEG membrane surface with a needle (4.3 ± 1.1 mg cm^{-2}). This deposition step was

performed in less than 20 seconds to limit the polymerization of the glue prior to its contact with tissues.

2.4.5. Area density of the coating. Films were weighed before and after coating using an analytical scale. The mass of coating per unit area m_c was given by $m_c = (M_a - M_b)/S$, where M_a is the mass of the coated film, M_b is the mass of the bare film, and S is the coated area.

2.4.6. Scanning electron microscopy (SEM). The surface of the coated films was characterized using scanning electron microscopy (SEM) on a FEI Nova NanoSEM 450 apparatus operating at an accelerating voltage of 2 kV. Dry samples were sputter coated with a 2 nm layer of gold/palladium. Observations were performed with a secondary electron TLD detector.

2.4.7. Image analysis. Image analysis was performed using the ''measure'' function of ImageJ software. The size of the nanoparticle aggregates was evaluated by measuring randomly selected aggregates (N = 280) on 5 different SEM images. The height of tissue deformation during peeling (see Fig. S2, ESI†) was assessed by analyzing 4 randomly selected snapshots of the peeling profile for each condition (PEG film, NP-coated film, and PEG coated with cyanoacrylate). At least 10 separate height measurements were made for each image (shown by the white arrows in Fig. S2, ESI†).

2.5. *Ex vivo* adhesion measurements

2.5.1. Preparation of PEG ribbons. Rectangular ribbons with 10-cm length, 1-cm width and 1-mm thickness were cut from PEG films. For experiments with various initial swelling ratios, the ribbons were swollen in ultrapure water at the desired ratio Q and left to equilibrate in a sealed container for a minimum of 4 hours prior to testing to ensure homogeneous distribution of water throughout the film thickness.

2.5.2. Preparation of liver substrate and deposition of ribbons. Rectangular liver samples with typical dimensions 120 mm × 30 mm × 10 mm were cut from liver lobes using a sharp knife. The surface of the parenchyma was exposed to air on the top face and the bottom face was glued onto a flat holder using cyanoacrylate glue. Uncoated or coated PEG ribbons were deposited at the surface of the liver samples within 10 ± 2 min after removal of the tissues from storage at 4 °C. For rehydrated livers, ribbon deposition occurred 10 ± 2 min after the end of the tissue swelling period in physiological serum. Pressure was applied repeatedly with one finger during the first minute of contact over the whole contact area while measuring the force with a weighing scale. A maximum force of 6 N was applied at each finger pressure, which corresponds to 80 ± 50 kPa. The ribbons were left on the liver for different contact times ranging from 5 to 30 min prior to peeling. The minimum contact duration is 5 minutes as it is the time required to install the system (PEG film in contact with liver substrate) in the tensile test apparatus before starting the measurement.

Peeling experiments were also performed on the liver capsule (the liver external collagenous membrane). For that, rectangular samples were cut from superficial liver tissues and immersed twice for 30 s in physiological serum. This gentle washing not only removed traces of coagulated blood that may affect adhesive properties but also ensured reproducible wetting of the tissue surface. Then, 1 min after the second tissue immersion in physiological serum, the bottom face of the liver sample was glued onto a flat holder with the capsule surface exposed to air on the top face. Uncoated or coated dry PEG films were deposited on the surface of the capsule in the same way as for parenchyma samples.

2.5.3. Peeling experiment. Peeling experiments were performed on a tensile test apparatus (All Around, Zwick) equipped with a 90° peeling device and a 10 N load cell. All peeling experiments were performed at 1 mm s^{-1}. The system was synchronized with video cameras to record side and front views of the peeling zone. The peeling force was systematically corrected by subtracting the weight of the lifted ribbon. The corrected force was given by $F = F^* - \rho d$ where F^* is the raw peeling force as measured by the cell force, d is the displacement and ρ is the linear mass of the ribbon. In all the work, the normalized corrected peeling force, F/w, is used, where w is the width of the peeled ribbon.

2.5.4. Calculation of adhesion energy. In each experiment, a steady state was reached with a constant peeling profile and a peeling angle equal to 90° after the first 10 to 20 mm of displacement. According to the theory of elastic peeling of a thin film,[29] the adhesion energy for each peeling experiment was calculated as $G = \langle F \rangle / w$ where $\langle F \rangle$ is the value of the corrected force averaged over the steady state peeling sequence.

2.6. Characterization of liver hydration

2.6.1. Measurement of liver water content. To evaluate the quantity of water present in the tissues, small liver samples (2–4 cm^3) were dried at 40 °C under vacuum until stabilization of their mass (less than 5 mg variation between two consecutive 4 h measurements). The water weight fraction H was given by $H = (M_i - M_{dry})/M_i$ where M_i is the initial sample mass and M_{dry} is the sample mass after drying. The liver samples used for these measurements were cut out from the same liver regions where peeling experiments were performed, and their initial mass was taken at the same time as the deposition of the hydrogel ribbons on tested tissues so as to reliably replicate hydration conditions found in the tested tissues.

2.6.2. Liver rehydration by swelling. Drained liver parenchyma samples were rehydrated by immersion in physiological serum (NaCl, 9 g L^{-1}) at room temperature. Prior to immersion, the volume V, the surface A and the initial mass M_i of each sample was measured. After a certain immersion time, the samples were removed from the serum and precociously shaken to remove excess superficial liquid after which the swollen mass M_s was measured. The swollen sample was subsequently dried after the method detailed above to yield the dry mass, M_{dry}. As demonstrated previously,[17] the liquid uptake during immersion is contained in a superficial tissue layer corresponding to the first layer of lobules exposed to the surface. Accordingly, the superficial water weight fraction H of rehydrated samples was assessed as follows:

$$H = 1 - \left[\frac{1}{1 - H_0} + \frac{\Delta M}{M_{dry}}\left(\frac{V}{Ab}\right)\right]^{-1} \quad (1)$$

where $H_0 = (M_i - M_{dry})/M_i$ is the water weight fraction prior to immersion, $\Delta M = (M_s - M_i)$ is the water uptake after immersion, and b (0.9 mm) is the characteristic half-size of one porcine lobule.

2.7. Assessment of the wetting of the PEG–tissue interface

Following a previously developed model,[17] the wetting state of the interface between the liver surface and the PEG film surface at the moment of peeling was characterized by the ratio v_{abs}/v_{free} where v_{abs} is the volume per unit surface of water absorbed by the PEG film at the time of peeling and v_{free} is the volume per unit surface of free water available in the superficial tissues before peeling. For each peeling experiment, v_{abs} was measured by weighing the mass of the PEG ribbon before and after peeling. It is then simply given by $v_{abs} = \Delta M/\rho A$ where ΔM is the mass uptake of the ribbon, ρ is the water density and A is the contact area. The value of v_{free} was calculated from the measured water weight fraction of the liver sample H as follows:

$$v_{free} = \frac{l_0}{2}\left[1 - (1 - \Phi_0)\left(\frac{1 - H}{1 - H_0}\right)\right]\left(\frac{1 - H_0}{1 - H}\right)^{1/3} \quad (2)$$

where Φ_0 is the porosity of lobular tissues corresponding to the volume fraction typically occupied by blood in mammalian livers under physiological conditions (taken to be equal to 0.3),[30,31] l_0 is the lobule characteristic size (taken to be equal to 1.75 ± 0.10 mm in the case of adult pork specimen (drained liver) and to be 1.28 ± 0.10 for a 3 month old specimen (fresh liver))[24] and H_0 is the water weight fraction in liver tissues under physiological conditions (taken to be equal to the average water weight fraction measured in the 4 most hydrated freshly dissected livers, H_0 = 79 ± 1%).

2.8. Optical microscopy for post-peeling observations

Bright field micrographs of the ribbons after the peeling experiments were performed on a Leica DMRXE microscope in transmission mode. Fluorescent micrographs of the PEG film and liver surfaces after peeling were carried out on a DMi8 Video microscope (Leica Microsystems) in reflection mode using a GFB filter (excitation wavelength: 470/40 nm, dichroic mirror: 495 nm, emission wavelength: 525/50 nm).

2.9. Statistical analysis

Statistical analysis was carried out on adhesion energies obtained using peeling experiments in the presence and absence of NP-coating. A Shapiro Wilk test was first performed on each population of data to determine if it follows a normal distribution. As normality was verified for all studied populations, an unpaired t-test was used to establish statistical significance. Statistical significance was accepted at the level of $p < 0.05$.

3. Results and discussion

3.1. Effect of tissue hydration

A powder consisting of microscopic aggregates of silica NPs was obtained from a solution of spherical silica nanoparticles with a diameter of 30 nm. Coated PEG films were obtained by brush spreading a given amount of this powder (4 mg cm^{-2}) as illustrated in Fig. 1(A). In this process, the PEG surface was saturated with aggregates and the excess powder was removed with a brush until a reproducible area density of 0.8 ± 0.2 mg cm^{-2} was achieved (Fig. 1(B)). SEM observations showed that the coatings were composed of a layer of microscopic polygonal aggregates as shown in Fig. 1(C). Image analysis indicated that the distribution in aggregate size followed a log-normal law with an average size $\langle D_{agg} \rangle$ of 5.0 μm and a standard deviation of 2.9 μm (Fig. 1(D)). The majority of those aggregates (~80%) were sufficiently adsorbed to the PEG film to resist washing in water for several hours, as shown in a previous study.[19]

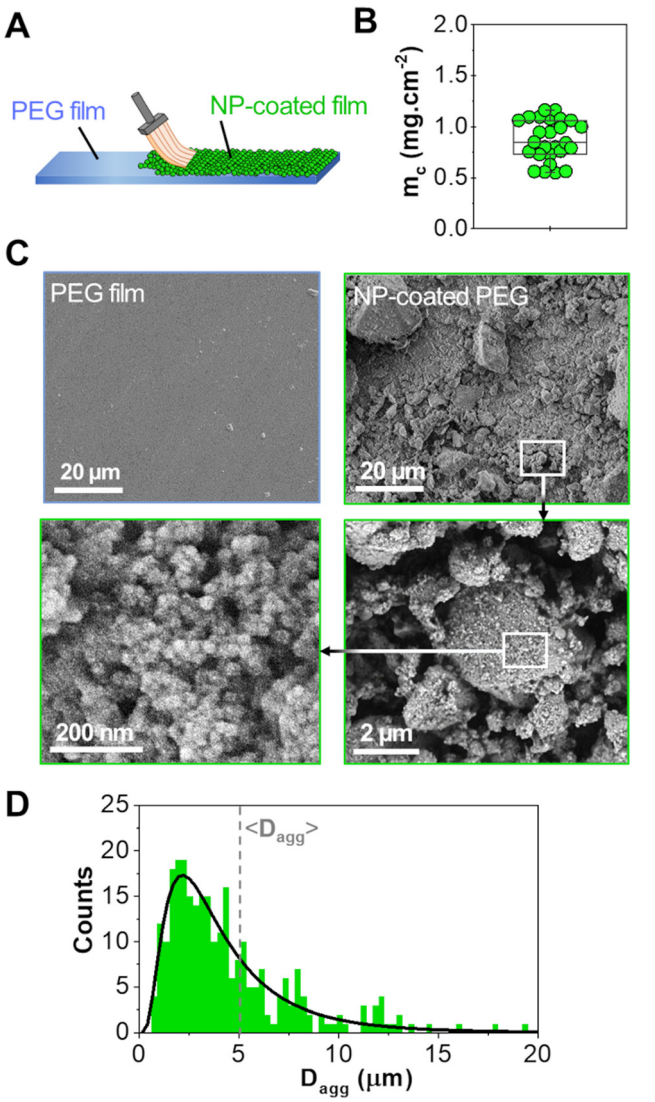

Fig. 1 NP coating characteristics. (A) Schematic representation of the NP coating deposition on a bare PEG film. (B) Area density of coatings (m_c) measured on multiple samples. (C) SEM images of a bare PEG film (top left corner) and a coated PEG film with different magnifications. (D) Distribution of the aggregate diameters (D_{agg}) following a lognormal law (black curve) and with an average value $\langle D_{agg} \rangle$ around 5 μm (data obtained from the measurements of about 300 aggregates on SEM images).

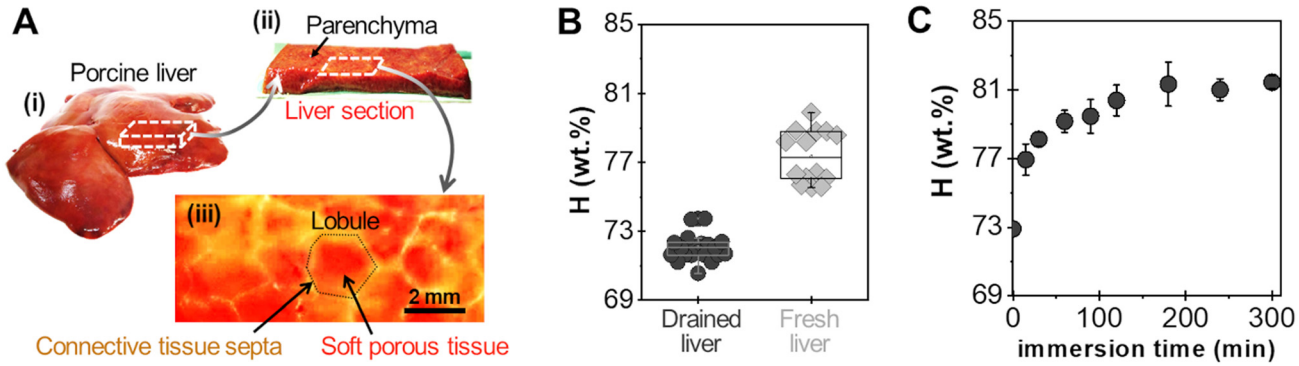

Fig. 2 Structure and hydration of porcine liver internal tissues. (A) Liver sample harvesting and surface: (i) whole liver, (ii) section of liver parenchyma, and (iii) photograph of the surface of a liver section displaying lobular structures. (B) Water weight fraction in drained and freshly dissected livers. Each point corresponds to one tissue sample taken from several drained livers (n = 7) and freshly dissected livers (n = 9). (C) Superficial water weight fraction as a function of immersion time in saline water for drained liver samples (n = 3–5 liver samples per data point).

For adhesion experiments, sections of porcine liver were cut to expose a flat surface of parenchyma, as represented in Fig. 2(A). The water weight fraction, H, of the liver tissue was varied by using two types of liver samples as shown in Fig. 2(B): (i) freshly dissected liver samples (n = 9), referred to as ''fresh liver'', for which H ranges from 76 to 80 wt% depending on the blood loss experienced by the tissues during dissection; (ii) butcher liver samples (n = 7), referred to as ''drained livers'', which contain less fluid (H = 72 ± 1 wt%). For some drained liver samples, the surface of the parenchyma was rehydrated just before adhesion measurement by immersion in physiological serum (NaCl 9 g L^{-1}) for various durations. This rehydration process was shown to be confined in the first layer of lobules exposed at the liver surface.[17] The local values of H near the surface of the rehydrated tissue were assessed to vary from 73 to 81 wt%, as shown in Fig. 2(C).

Adhesion was measured by 90° peeling of PEG ribbons deposited on those liver sections, as depicted in Fig. 3(A). Typical force displacement curves obtained for the peeling after 5 min of contact are shown in Fig. 3(B) in the case of fresh liver parenchyma with a moderate water content (H = 76 ± 0.5 wt%) for bare and NP-coated PEG films. These results are compared to those obtained with PEG films glued with a comparatively much larger quantity of medical grade cyanoacrylate glue, GLUture® (4.3 ± 1.1 mg cm^{-2}). For the bare PEG film, a normalised peeling force of 3.3 ± 1.1 N m^{-1} was reached in the steady state. During peeling, liver tissues were slightly lifted by the gel as illustrated in Fig. 3(C)-(i) and detachment was located at a height of 1.7 ± 0.3 mm above the plane of the hydrogel–tissue interface (Fig. S2, ESI†). For the NP-coated PEG film, the normalized peeling force was three times higher with an average value of 10.3 ± 4.8 N m^{-1}. This came along with a

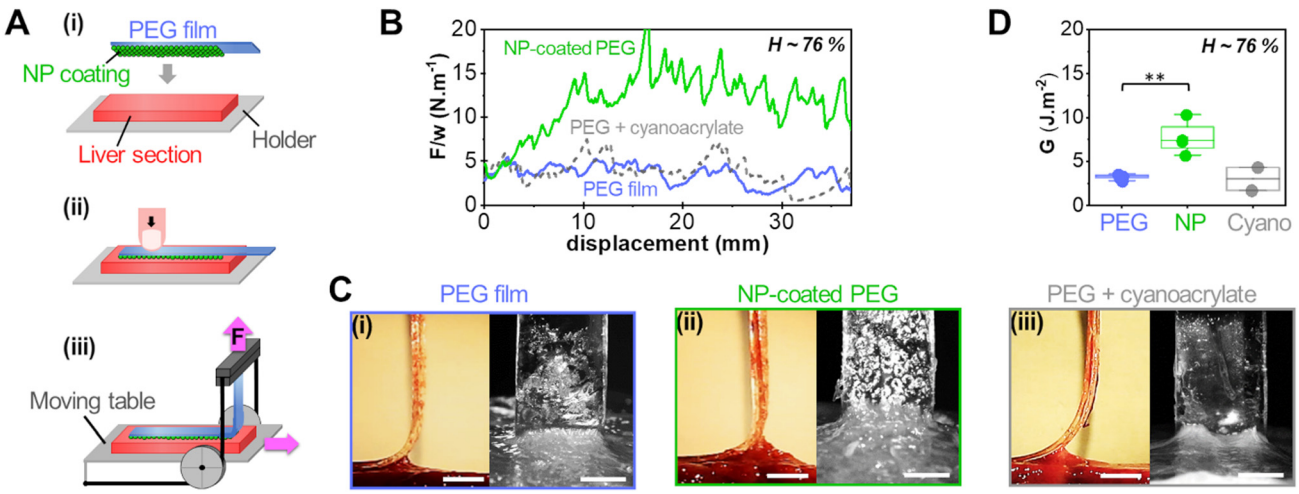

Fig. 3 Adhesion on moderately hydrated fresh liver tissues. (A) Schematic drawing of the 90° peeling protocol: (i) deposition of a NP-coated PEG film on a liver section, (ii) manual pressure application, and (iii) peeling of the film from the liver surface with a 90° geometry. (B) Normalised peeling force as a function of peeling displacement for a bare PEG film, a NP-coated PEG film and a PEG film covered with cyanoacrylate glue on a fresh liver sample with water weight fraction H = 76 ± 0.5 wt%. (C) Corresponding side and front views during steady state peeling for the tests shown in (B). (D) Adhesion energies G obtained with bare PEG films, NP-coated PEG films and PEG films covered with cyanoacrylate glue on different liver parenchyma samples with a water weight fraction of 76 ± 0.5 wt% (**$p < 0.005$; scale bar: 5 mm).

larger tissue deformation at the detachment front, lifting the liver 3 ± 1 mm above the hydrogel–tissue interface, as seen in Fig. 3(C)-(ii) and Fig. S2 (ESI†). By comparison, the PEG ribbon glued with cyanoacrylate glue led to an average peeling force of 4.3 ± 2.4 J m^{-2} and a detachment height of 1.0 ± 0.7 mm (Fig. 3(C)-(iii) and Fig. S2, ESI†). This low adhesion value is consistent with the poor adhesive performance generally reported for surgical cyanoacrylate glues under hydrated conditions due to the rapid formation of a hard and brittle interfacial film.[21,32]

The adhesion energy, G, was estimated from the averaged normalised peeling force using Kendall's model for elastic peeling (see the materials and methods section). Fig. 3(D) shows the values of G obtained on several sections of a moderately hydrated parenchyma (H = 76 ± 0.5 wt%) for bare PEG films, NP-coated PEG films and PEG films with cyanoacrylate glue. The adhesion of NP-coated films was systematically and significantly stronger than that of bare PEG films (p = 0.0013). The average adhesion energy obtained with the NP coating was 7.7 ± 1.9 J m^{-2} which represents a 2- to 3-fold increase as compared to the bare PEG films (3.2 ± 0.3 J m^{-2}) and the cyanoacrylate glue (2.9 ± 1.9 J m^{-2}).

Typical results of peeling experiments on highly hydrated liver tissues are shown in Fig. 4. For the most hydrated fresh liver samples (H = 79.9 ± 0.9 wt%), the peeling force and adhesion energy after 5 min of contact were greatly reduced as shown in Fig. 4(A) for the bare PEG (0.8 ± 0.2 J m^{-2}) and NP-coated PEG (1.3 ± 0.3 J m^{-2}). This loss of adhesion was amplified when peeling on even more hydrated tissues (H = 81 ± 1 wt%) obtained by rehydration of drained liver samples (Fig. 4(B)). On these tissues, the average peeling force for both the bare and NP-coated PEG films was of the order of capillary forces (<0.5 N m^{-1}). Accordingly, the side and front views of the detachment zone indicate the presence of a lubricated interface with a meniscus moving as the peeling proceeds (Fig. 4(C)). Hence, on these very hydrated substrates, the NP coating did not produce any adhesive effect.

The sensitivity of adhesion to liver hydration can be rationalized by considering the competition between the wetting of the interface due to the capillary rise of the free liquid contained in the tissue and the draining of the interfacial liquid by the swelling hydrogel film. As reported in a previous study on bare PEG films,[17] this competition is well described by the ratio v_{abs}/v_{free} between the volume of liquid absorbed by the PEG film at the moment of peeling (v_{abs}) and the volume of free liquid contained in the superficial tissue before contact (v_{free}). At the moment of peeling, two situations can arise: ($v_{abs}/v_{free} < 1$) some liquid remains at the interface and the contact is lubricated, therefore preventing adhesion; ($v_{abs}/v_{free} > 1$) all the interfacial liquid has been drained and adhesive contact has been achieved.

In the present work, v_{abs} was measured by weighing the film mass uptake immediately after peeling and v_{free} was calculated from histological data and from the measured tissue water weight fraction H (see the materials and methods section). The values of v_{abs} and v_{free} were varied by adjusting experimental

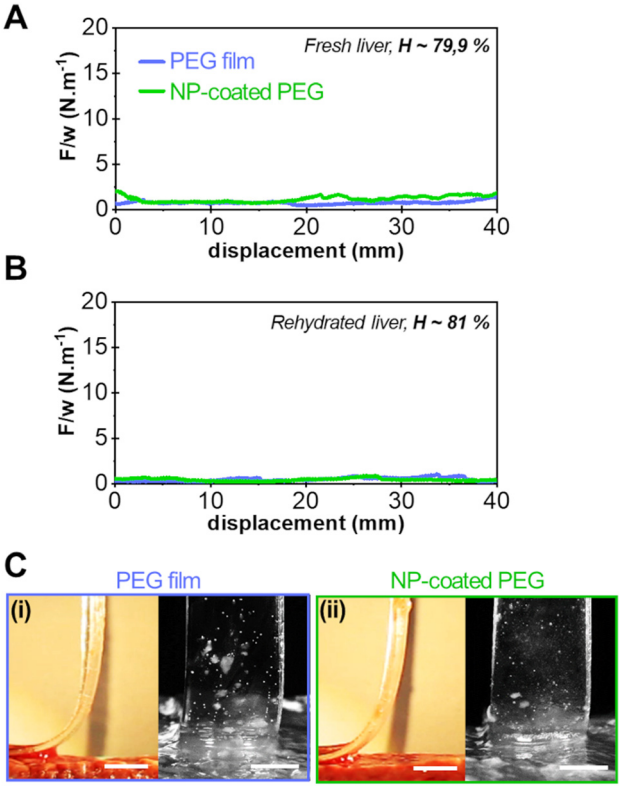

Fig. 4 Adhesion on highly hydrated liver tissues. (A) Normalised peeling force as a function of peeling displacement for a bare PEG film and a NP-coated PEG film on a fresh liver sample with a water weight fraction H = 79.9 ± 0.5 wt%. (B) Same as (A) on rehydrated drained liver parenchyma with a water weight fraction H = 81 ± 1 wt%. (C) Corresponding side and front views during peeling of bare PEG (i) and NP-coated PEG film (ii) on rehydrated drained liver parenchyma with a water weight fraction H = 81 ± 1 wt% (scale bar: 5 mm).

conditions such as the initial swelling ratio of the PEG film (Q), the initial water weight fraction of the liver substrate (H) and the duration of contact between the film and the tissue (Δt). The resulting values of adhesion energy G are plotted as a function of v_{abs}/v_{free} in Fig. 5(A) and (B) for the bare PEG and the NP-coated PEG films, respectively. For both systems, the transition from a lubricated contact (open symbols) to an adhesive contact (full symbols) occurs for $v_{abs}/v_{free} \approx 1$, suggesting that adhesive binding is only established once all the interfacial fluid has been drained. In the adhesive regime ($v_{abs}/v_{free} > 1$), NP-coated PEG films produced higher adhesion energies than bare PEG films. In particular, the maximum energy recorded for NP-coated films was 13 J m^{-2} for v_{abs}/v_{free} = 1.5, corresponding to a 2.2-fold increase when compared to uncoated films under the same conditions. More generally, the presence of the NP-coating resulted in a statistically significant increase in adhesion energy ($p < 0.001$) when examining all the data obtained under conditions for which $v_{abs}/v_{free} > 1$ (Fig. 5(C)).

A closer comparison between the data for the bare and the NP-coated films reveals that the transition from the lubricated to the adhesive regime is shifted to more hydrated conditions

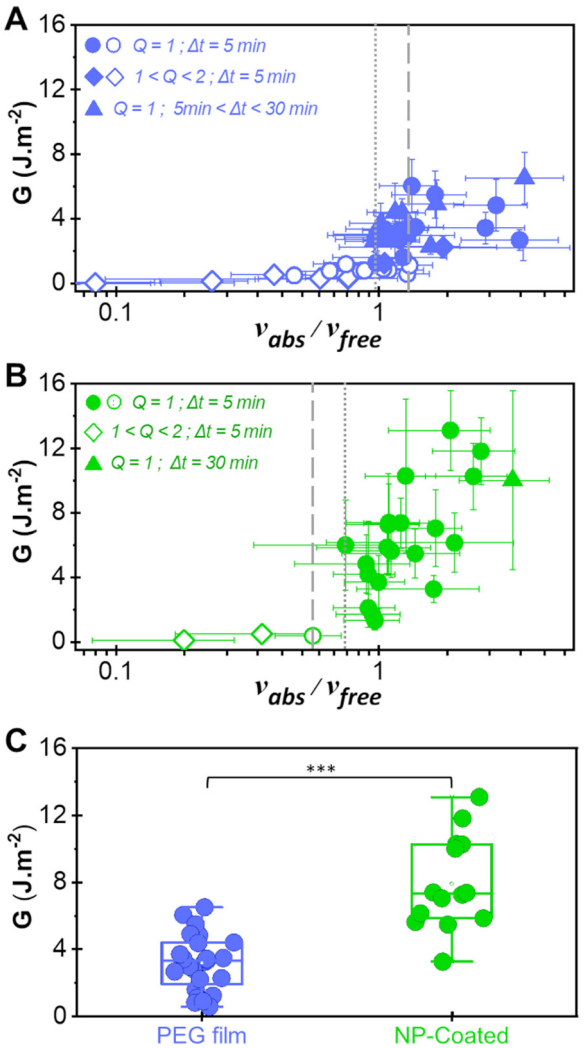

Fig. 5 Adhesion as a function of interfacial wetting. (A) and (B) Adhesion energy as a function of the ratio v_{abs}/v_{free} describing the competition between interfacial wetting and draining for bare PEG films (A) and NP-coated PEG films (B). Circles correspond to peelings performed with dry PEG ribbons after 5 min of contact, diamonds to peelings performed with partially swollen PEG ribbons after 5 min of contact and triangles to peeling performed with dry PEG ribbons after various contact times. Open symbols correspond to lubricated peeling and full symbols to adhesive peeling. The data in (A) were reproduced and modified with permission from ref. 17, copyright 2019 National Academy of Sciences. (C) Adhesion energy obtained with bare PEG and NP-coated PEG films under conditions for which $v_{abs}/v_{free} > 1$ (***$p < 0.001$).

in the presence of the NP coating. For the bare films, the adhesive regime starts at $v_{abs}/v_{free} = 1.0 \pm 0.3$ and there is an overlap of lubricated and adhesive data between 1.0 and 1.3 (the space between the dotted and dashed lines in Fig. 5(A)). For the NP-coated films, the first adhesive peeling was obtained for $v_{abs}/v_{free} = 0.8 \pm 0.4$ (dotted line in Fig. 5(B)) and no lubricated peeling was observed above $v_{abs}/v_{free} = 0.6 \pm 0.2$ (dashed line in Fig. 5(B)).

This improved adhesive performance of NP-coated PEG films under moderately hydrated conditions can be attributed to the ability of the porous NP aggregates to rapidly drain the interfacial liquid by capillarity. In the case of a bare PEG film, the draining of interfacial liquid occurs due to the swelling of the PEG network.[17] This process is limited by the diffusive dynamics of the PEG chains and is much slower than the capillary rise of free fluid coming from the microscopic interstices of the parenchyma. To quantify this difference, let us consider the characteristic time t^* that is necessary for fluids to rise through the tissue microporosities and wet the tissue surface with a layer of thickness h^*. From the Lucas and Washburn law, t^* is expressed as follows (see the ESI† for details):[33,34]

$$t^* = \left(\frac{h^*}{\Phi}\right)\left(\frac{2\eta}{\gamma R \cos\theta}\right) \quad (3)$$

where Φ is the medium porosity, γ is the surface tension of the liquid, R is the radius of the capillary tubes, θ is the contact angle and η is the liquid viscosity. Taking appropriate values for the porcine liver parenchyma, eqn (3) indicates that it takes approximately 0.02 ms for a 10-μm-thick fluid layer to form at the tissue surface. In contrast, swelling measurements indicate that the absorption of the same fluid layer by the dry bare PEG film takes about 2 s (Fig. S1, ESI†). Hence, the interfacial draining by osmotic swelling is about five orders of magnitude slower than the capillary wetting from the tissue. For the bare PEG film, it is thus expected that the interface remains lubricated as long as v_{free} is superior to v_{abs}.

In the presence of a NP coating, the draining of the interfacial liquid may occur in two stages. In the first stage, immediately after contact with wet tissues, a certain amount of liquid may be quickly absorbed by capillary rise inside the inter- and intra-aggregate porosities of the coating. In the second stage, once the pores of the coating are filled, the draining of the interfacial liquid is governed by the slow swelling kinetics of the PEG network, like in the case of the bare film. Eqn (3) can be employed to calculate the characteristic time necessary for a 10-μm-thick fluid layer to be absorbed through the nanoparticle coating porosities. In this case, the medium porosity Φ was evaluated from the structural parameters of the coating with the following equation (see the ESI† for details):

$$\Phi = \frac{\langle D_{agg}\rangle - m_c/d_{SiO_2}}{\langle D_{agg}\rangle} \quad (4)$$

where $\langle D_{agg}\rangle$ is the average diameter of nanoparticle aggregates (5 μm), m_c is the surface density of the coating (0.8 mg cm^2) and d_{SiO_2} is the density of amorphous silica ($d_{SiO_2} = 2.3$). As regards parameter R in eqn (3) (the average radius of the coating porosities), its value can be roughly estimated from SEM images to be in the order of 0.1 to 10 μm (see Fig. S3, ESI†). With those coating parameters, we find that the characteristic time to drain a 10-μm-thick fluid layer into the coating is in the order of 0.002 to 0.2 ms, which is comparable to the time needed for the wetting of the tissue surface (0.02 ms). Therefore, in the first moments of contact, a rapid draining of the tissue by the particle coating may occur and allow the adsorption of tissue macromolecules onto the particles. This particle

bridging may then resist the wetting of the interface endured during the second stage of slower water absorption. This is consistent with previous observations showing that silica NP aggregates adsorbed on a PEG surface are able to resist extensive washing with water.[19] This mechanism would explain why adhesive peeling was achieved with an NP-coating, even when all the free fluid wetting the interface has not been completely absorbed into the PEG film ($v_{abs}/v_{free} < 1$).

Increasing the contact time up to 30 min produced the highest adhesion energies for both the bare and NP-coated films, as shown by triangle symbols in Fig. 5(A) and (B), respectively. For those longer contact times, higher values of v_{abs} were measured suggesting a stronger local dehydration of the tissue, which is more favourable to macromolecular adsorption and viscous dissipation during peeling. In such *ex vivo* experiments, much longer contact times may be needed to achieve equilibration and rehydration of the interface that could lead to a decrease in adhesion. For *in vivo* adhesion, rehydration is expected to occur much faster due to the continuous vascularization of tissues, therefore favouring the lubrication of the contact. This is consistent with the very low pull-out strength measured during *in vivo* experiments on the liver capsule with the same NP-coated films for 10 min and 40 min contact times.[19]

3.2. Effect of local tissue composition

When NP-coated films were peeled from the surface of liver parenchyma in the adhesive regime ($v_{abs}/v_{free} > 0.75$), transfer of matter was observed as shown in Fig. 3(B)-(ii) and Fig. 6(A). On the one hand, some NP-aggregates transferred from the PEG film to the liver surface and on the other hand, some liver fragments transferred to the PEG film surface. These transfers displayed a patterned structure resembling the lobular architecture of the liver parenchyma, as presented in Fig. 2(A)-(iii). In a series of experiments, a small amount of fluorescent silica particles (1 wt%) was included in the NP aggregates composing the coating to better characterize these transfers by means of bright field and fluorescent microscopy. The adhesive properties of these fluorescent coatings were tested and found to be very similar to those presented above with non-fluorescent coatings (Fig. S4, ESI†).

After peeling of PEG films covered with this fluorescent coating, observations of the film surface show the deposition of reddish tissue patches, as seen on macroscopic images and bright field micrographs in Fig. 6(B) and (C). In the areas where liver tissue was transferred, fluorescence microscopy revealed that the NP coating was still present on the PEG surface as shown in Fig. 6(D) (see Fig. S5, ESI† for larger scale mapping). The intensity of fluorescence recorded in these areas was comparable to the one observed on the NP-coated film before peeling (Fig. S6B, ESI†). In contrast, the areas between the transferred tissue fragments exhibited a negligible fluorescence, similar to that of the bare PEG membrane (Fig. S6A, ESI†). In these areas, the NP aggregates were removed from the PEG surface during peeling.

Observations of the liver surface after peeling showed a patterned deposition of NP aggregates (Fig. 6(E)) forming a negative footprint of the pattern observed on the corresponding coated PEG film. This transfer seemed to occur almost exclusively on the connective tissues constituting the collagen-rich walls of the liver lobules (Fig. 6(F)). The deposition of NP-aggregates on the liver tissues was further confirmed by fluorescent microscopy, as NP-aggregates are visible on fluorescent micrographs and emit light in an intensity range for which the

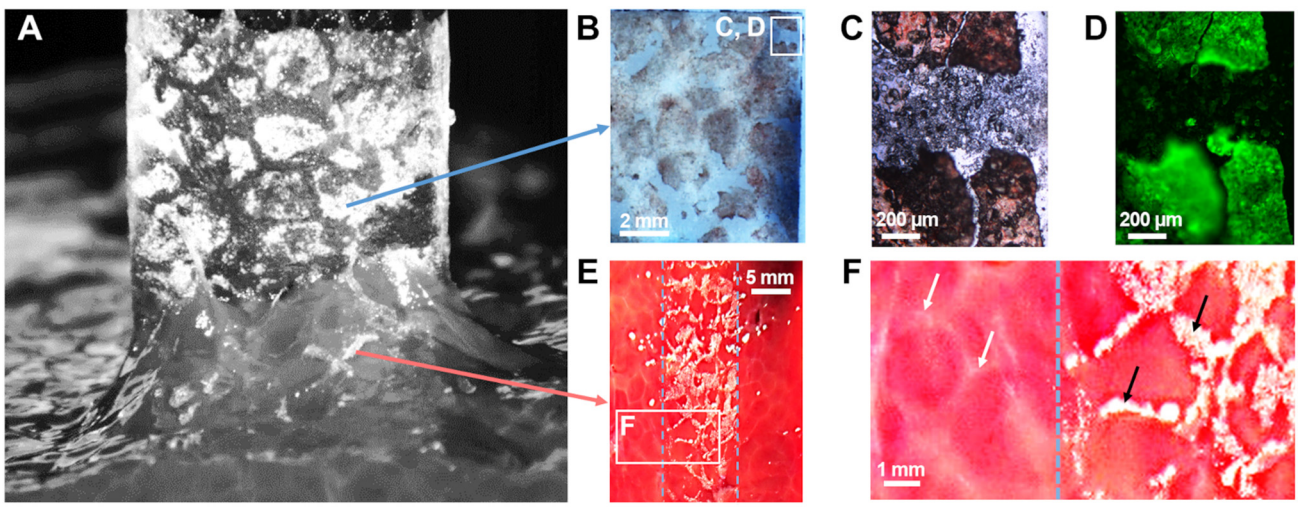

Fig. 6 Microscopic observations of the tissue and film surfaces after peeling. (A) Front view of the detachment zone during peeling of a PEG film coated with fluorescent NP aggregates in the adhesive regime ($v_{abs}/v_{free} > 1$). (B)–(D) Observations of the coated PEG film surface after peeling: (B) photograph of the PEG film displaying patterned tissue deposition; (C) bright field micrograph of the region between two transferred tissue deposits; (D) fluorescent micrograph of the same region. (E) and (F) Observations of the liver surface after peeling: (E) photograph of the tissue surface after peeling showing the area in contact with the coated-PEG ribbon (area delimited by the blue dashed lines); (F) higher magnification observation close to the edge of the peeled area showing the correspondence between the lobular walls and the transferred particle pattern (white arrows showing lobular walls, and black arrows showing deposited particle "patches").

liver auto-fluorescence is almost entirely suppressed (Fig. S7, ESI†).

These results show a strong correlation between the local detachment mechanisms and the local composition of the tissue. We propose a microscopic picture for the detachment process that accounts for the histology of the liver parenchyma, as depicted in Fig. 7. The surface of the porcine liver parenchyma displays a cellular structure consisting of hepatic lobules separated by walls composed of collagen-rich connective tissues. We assume here that peeling was performed in the adhesive regime for which the interstitial liquid was drained and macromolecules composing the tissue could adsorb on the NP coating (Fig. 7(A)). During peeling, the tissues are pulled upwards by the PEG film which first causes a cohesive rupture of the more fragile lobule internal tissues (Fig. 7(B)). As peeling proceeds, the collagen-rich lobular walls can resist higher tensile stresses and experience a larger deformation as evidenced by the appearance of elongated strands at the peeling front (white arrows in Fig. 7(B)). Eventually, the NP aggregates adsorbed to the lobular walls detach from the PEG surface and get transferred to the tissue surface (Fig. 7(C)). After detachment, the PEG film displays patches of coating covered with fragments of the soft tissues originating from the interior of the liver lobules while the tissue surface presents a patterned deposition of NP aggregates located on top of the lobular walls.

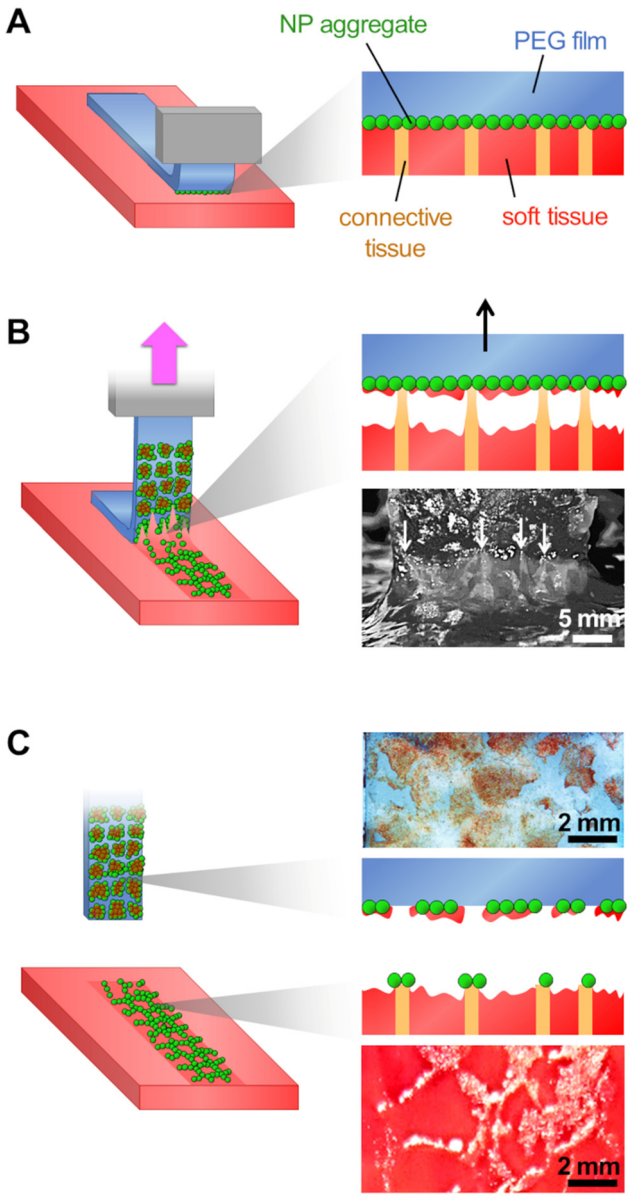

Fig. 7 Microscopic picture of the mechanisms occurring during adhesive peeling. (A) Before peeling, the NP-coated PEG film is in contact with the fibrous connective tissues and soft tissues of the liver parenchyma. (B) Upon peeling, in the detachment zone, soft tissues are rapidly torn off and form tissue patches on the PEG film. In contrast, fibrous connective tissues adsorbed onto the coating resist the peeling and stretch thereby creating the main contribution to the peeling force. White arrows on the front view indicate regions where adsorbed connective tissues are deformed by the peeling process. (C) After peeling, the adhesion between the liver connective tissues and the particle coating ultimately leads to the detachment of the NP aggregates transferred along the lobular walls of the tissue.

From this microscopic picture, it appears that the main contribution to the measured peeling force arises from the adhesion of the NP-coating to the collagen-rich lobular walls of the liver parenchyma. The cohesive strength of the soft cellular tissues of the lobule interior is clearly lower than the strength of the adhesion with the NP-coating. During peeling, the cohesive rupture inside the lobule occurs early while binding is maintained in the areas in contact with the lobular walls which stretch until NP aggregates detach from the PEG surface. As compared to the soft lobule interior, the collagen-rich lobular walls are much tougher materials due to the ability of collagen fibrils to withstand large tensile stresses, up to 0.6 GPa according to Shen *et al.*[35] Our microscopic observations did not allow us to determine whether the NP aggregates desorbed from the gel or whether there was a cohesive rupture in the PEG gel underneath the particles. Nevertheless, these experiments indicate that a strong binding was established between collagen-rich tissues and NP aggregates. This is in line with previous reports highlighting the affinity between collagen and silica resulting from a combination of attractive electrostatic interactions and hydrogen bonds.[36,37] More generally, these results suggest that such silica-coated films may adhere rather strongly to other tissue types displaying a collagenous lining.

To support this hypothesis, peeling experiments were performed on the liver capsule (the liver external membrane) that is composed of a collagenous basal membrane. Liver capsules were soaked in saline water in a controlled way to mimic the physiological wetting of the liver. After 5 min of contact on the so-prepared liver capsule, we showed in a previous study that the interface is in the adhesive regime ($\nu_{abs}/\nu_{free} > 1$).[17] Fig. 8 shows typical peeling experiments conducted with a bare PEG film and a NP-coated PEG film on the capsule of fresh liver samples. The presence of the silica NP-coating produces a very significant increase in adhesion energy as compared to the bare PEG film, as shown in Fig. 8(A). The adhesion energy ($\sim$12 J m^{-2}) is similar to what was obtained on the parenchyma. However, unlike adhesion onto the parenchyma, the peeling front of the NP-coated PEG on the liver capsule displays

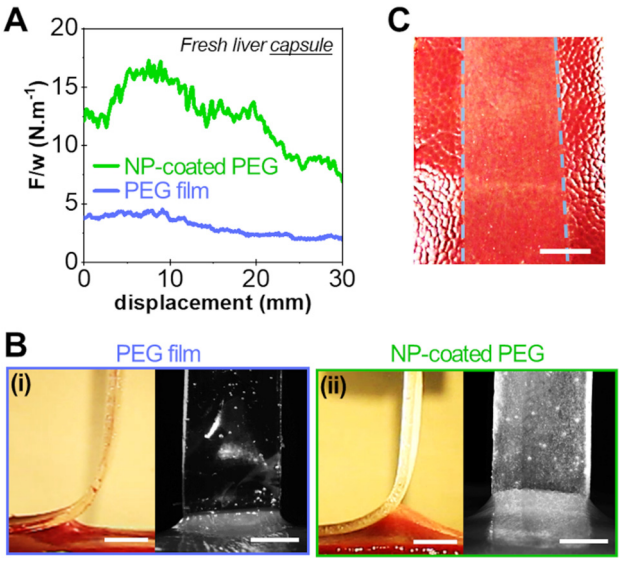

Fig. 8 Adhesion on the liver collagenous capsule. (A) Normalised peeling force as a function of peeling displacement for a bare PEG film and a NP-coated PEG film on a fresh liver capsule sample. (B) Corresponding side and front views during peeling of bare PEG (i) and NP-coated PEG film (ii) on a fresh liver capsule sample. (C) Photograph of the liver capsule surface after peeling with a NP-coated PEG film. The area in contact with the coated-PEG ribbon (indicated by the blue dashed lines) displays a relatively uniform deposition of NP aggregates after peeling (scale bar: 5 mm).

a homogeneous profile: the detachment height is constant across the width of the film (Fig. 8(B)). A transfer of silica particles is observed on the liver capsule covering homogeneously the contact area (Fig. 8(C)), like the transfer observed on the collagen-rich lobular walls of the parenchyma.

Conclusions

Model adhesion experiments using peeling on *ex vivo* liver parenchyma shed light on the interfacial phenomena governing the adhesion by particle bridging onto biological tissues. Firstly, the transport of fluid at the interface was found to be determinant for the establishment of an adhesive behaviour. Under highly hydrated conditions, for which interstitial fluids wet the interface and prevent molecular contact, no enhancement of adhesion by particle bridging was obtained. In contrast, under moderately humid conditions, the use of NP-coating yielded a statistically significant increase in adhesion and led to adhesive performances superior to that of cyanoacrylate glues. In addition, adhesion measurements with various tissue hydration levels showed that the capillary transport inside the porous coating might accelerate the draining of the interface at short times and facilitate the creation of an adhesive contact. This beneficial effect of the coating might be combined with other draining strategies including the patterning of surfaces[38,39] or the use of superabsorbent gels[17,18] to enhance tissue adhesion. Moreover, the use of highly dissipative films[21,40] could provide a way to increase the adhesion energy when an adhesive contact is produced. Secondly, these experiments showed that the detachment process depends on the local tissue composition, which determines the local adhesion strength. For a tissue surface as heterogeneous as the porcine liver parenchyma, the adsorption of the silica NP coating onto the tissue was strong enough to either lead to cohesive tissue rupture when in contact with soft cellular tissues or to a detachment of the NP particles from the PEG film when in contact with collagen-rich connective tissues. This understanding of microscopic interfacial processes, involving fluid transport and tissue-specific interactions, delivers new insights into the design of particle-bridging approaches as adhesives to biological tissues.

Conflicts of interest

There are no conflicts to declare.

Acknowledgements

We thank J. Legagneux (AP-HP) for the liver harvesting. Technological support from the Institut P-G de Gennes Program ANR-10-EQPX-34 as well as financial support from the Agence Nationale de la Recherche (ANR-18-CE19-0022-04 NanoBioTape), PSL University (PSL-Chimie-2014 HemoSoftChem), MINES Paris and ESPCI Paris are acknowledged. For the purpose of open access, the authors have applied a CC-BY public copyright licence to any Author Accepted Manuscript (AAM) version arising from this submission.

Notes and references

1 S. Rose, A. Prevoteau, P. Elziere, D. Hourdet, A. Marcellan and L. Leibler, *Nature*, 2014, **505**, 382–385.
2 M. C. Arno, M. Inam, A. C. Weems, Z. Li, A. L. A. Binch, C. I. Platt, S. M. Richardson, J. A. Hoyland, A. P. Dove and R. K. O'Reilly, *Nat. Commun.*, 2020, **11**, 1420.
3 J. S. Baik, S. A. Kim, D.-W. Jung, W.-S. Chae, C. Pang, S. H. Bhang, L. Corté and G.-R. Yi, *Chem. Mater.*, 2022, **34**, 584–593.
4 J.-H. Kim, H. Kim, Y. Choi, D. S. Lee, J. Kim and G.-R. Yi, *ACS Appl. Mater. Interfaces*, 2017, **9**, 31469–31477.
5 A. Meddahi-Pelle, A. Legrand, A. Marcellan, L. Louedec, D. Letourneur and L. Leibler, *Angew. Chem., Int. Ed.*, 2014, **53**, 6369–6373.
6 M.-M. Lu, J. Bai, D. Shao, J. Qiu, M. Li, X. Zheng, Y. Xiao, Z. Wang, Z.-M. Chang, L. Chen, W.-F. Dong and C.-B. Tang, *Int. J. Nanomed.*, 2018, **13**, 5849–5863.
7 K. Shin, J. W. Choi, G. Ko, S. Baik, D. Kim, O. K. Park, K. Lee, H. R. Cho, S. I. Han, S. H. Lee, D. J. Lee, N. Lee, H.-C. Kim and T. Hyeon, *Nat. Commun.*, 2017, **8**, 15807.
8 H. Wu, F. Li, S. Wang, J. Lu, J. Li, Y. Du, X. Sun, X. Chen, J. Gao and D. Ling, *Biomaterials*, 2018, **151**, 66–77.
9 M. T. Matter, F. Starsich, M. Galli, M. Hilber, A. A. Schlegel, S. Bertazzo, S. E. Pratsinis and I. K. Herrmann, *Nanoscale*, 2017, **9**, 8418–8426.

10 E. Palierse, M. Roquart, S. Norvez and L. Corté, *RSC Adv.*, 2022, **12**, 21079–21091.
11 Q. Zeng, K. Han, C. Zheng, Q. Bai, W. Wu, C. Zhu, Y. Zhang, N. Cui and T. Lu, *J. Colloid Interface Sci.*, 2022, **607**, 1239–1252.
12 S. Pourshahrestani, E. Zeimaran, N. A. Kadri, N. Mutlu and A. R. Boccaccini, *Adv. Healthcare Mater.*, 2020, **9**, 2000905.
13 Y. Liang, J. He and B. Guo, *ACS Nano*, 2021, **15**, 12687–12722.
14 J. Chen, D. Wang, L.-H. Wang, W. Liu, A. Chiu, K. Shariati, Q. Liu, X. Wang, Z. Zhong, J. Webb, R. E. Schwartz, N. Bouklas and M. Ma, *Adv. Mater.*, 2020, **32**, 2001628.
15 S. A. Mortazavi and J. D. Smart, *J. Controlled Release*, 1993, **25**, 197–203.
16 J. D. Smart, *Adv. Drug Delivery Rev.*, 2005, **57**, 1556–1568.
17 R. Michel, L. Poirier, Q. van Poelvoorde, J. Legagneux, M. Manassero and L. Corté, *Proc. Natl. Acad. Sci. U. S. A.*, 2019, **116**, 738.
18 H. Yuk, C. E. Varela, C. S. Nabzdyk, X. Mao, R. F. Padera, E. T. Roche and X. Zhao, *Nature*, 2019, **575**, 169–174.
19 R. Michel, M. Roquart, E. Llusar, F. Gaslain, S. Norvez, J. S. Baik, G.-R. Yi, M. Manassero and L. Corté, *ACS Appl. Bio Mater.*, 2020, **3**, 8808–8819.
20 N. Artzi, T. Shazly, A. B. Baker, A. Bon and E. R. Edelman, *Adv. Mater.*, 2009, **21**, 3399–3403.
21 J. Li, A. D. Celiz, J. Yang, Q. Yang, I. Wamala, W. Whyte, B. R. Seo, N. V. Vasilyev, J. J. Vlassak, Z. Suo and D. J. Mooney, *Science*, 2017, **357**, 378.
22 N. Artzi, A. Zeiger, F. Boehning, A. Bon Ramos, K. Van Vliet and E. R. Edelman, *Acta Biomater.*, 2011, **7**, 67–74.
23 L. Eberlova, A. Maleckova, P. Mik, Z. Tonar, M. Jirik, H. Mirka, R. Palek, S. Leupen and V. Liska, *J. Surg. Res.*, 2020, **250**, 70–79.
24 E. G. White, *J. Anat.*, 1939, **73**, 365–386.
25 P. M. Baptista, M. M. Siddiqui, G. Lozier, S. R. Rodriguez, A. Atala and S. Soker, *Hepatology*, 2011, **53**, 604–617.
26 E. D. Strange, M. P. Dahms, R. C. Benedict and J. H. Woychik, *J. Food Sci.*, 1985, **50**, 1484–1485.
27 B. J. Frisken, *Appl. Opt.*, 2001, **40**, 4087–4091.
28 D. Zhang, Z. Wu, J. Xu, J. Liang, J. Li and W. Yang, *Langmuir*, 2010, **26**, 6657–6662.
29 K. Kendall, *J. Phys. D: Appl. Phys.*, 1975, **8**, 1449–1452.
30 C. F. Rothe, in *Veins: Their Functional Role in the Circulation*, ed. S. Hirakawa, C. F. Rothe, A. A. Shoukas and J. V. Tyberg, Springer, Japan, Tokyo, 1993, pp. 90–97.
31 J. Schafer, M. S. D'Almeida, H. Weisman and W. W. Lautt, *Hepatology*, 1993, **18**, 969–977.
32 V. Bhagat and M. L. Becker, *Biomacromolecules*, 2017, **18**, 3009–3039.
33 R. Lucas, *Kolloid-Z.*, 1918, **23**, 15–22.
34 E. W. Washburn, *Phys. Rev.*, 1921, **17**, 273–283.
35 Z. L. Shen, M. R. Dodge, H. Kahn, R. Ballarini and S. J. Eppell, *Biophys. J.*, 2008, **95**, 3956–3963.
36 D. Eglin, T. Coradin, M. M. Giraud Guille, C. Helary and J. Livage, *Bio-Med. Mater. Eng.*, 2005, **15**, 43–50.
37 D. Eglin, G. Mosser, M.-M. Giraud-Guille, J. Livage and T. Coradin, *Soft Matter*, 2005, **1**, 129–131.
38 F. Meng, Q. Liu, Z. Shi, D. Tan, B. Yang, X. Wang, K. Shi, M. Kappl, Y. Lei, S. Liu and L. Xue, *Adv. Mater. Interfaces*, 2021, **8**, 2100528.
39 M. Li, J. Xie, Q. Dai, W. Huang and X. Wang, *J. Mech. Behav. Biomed. Mater.*, 2018, **78**, 266–272.
40 P. Karami, C. S. Wyss, A. Khoushabi, A. Schmocker, M. Broome, C. Moser, P.-E. Bourban and D. P. Pioletti, *ACS Appl. Mater. Interfaces*, 2018, **10**, 38692–38699.